Kinetics of Film Formation in Acrylic Latices Studied with Multiple-Angle-of-Incidence Ellipsometry and Environmental SEM

J. L. Keddie,* P. Meredith, R. A. L. Jones, and A. M. Donald

Polymer and Colloid Group, Cavendish Laboratory, Department of Physics, University of Cambridge, Madingley Road, Cambridge, CB3 0HE, United Kingdom

Received September 7, 1994; Revised Manuscript Received January 30, 1995[⊗]

ABSTRACT: A combination of multiple-angle-of-incidence ellipsometry (MAIE) and environmental SEM (ESEM) was used to characterize the microstructure of acrylic latices during all four stages of film formation, starting from an aqueous colloidal dispersion (Stage I) and evolving to a continuous coating having no internal solid–solid interfaces (Stage IV). Stage II is usually defined as a close-packed array with water-filled interstices, and Stage III is defined as a densely packed array of deformed particles. This analysis identified an additional stage, II*, intermediate to the conventionally defined Stages II and III. The onset of this new stage, which coincides with the development of optical clarity, occurs at nearly the same time (normalized by the final film thickness), regardless of the glass transition temperature (T_g) of the latex polymer. The duration of Stage II* and the kinetics of particle coalescence in Stage III, on the other hand, are a function of T_g. A latex with a T_g well below the ambient temperature can deform rapidly to fill the space left by the evaporation of water. A latex with a higher T_g cannot, and so air voids and surface roughness develop and persist over measurable times.

I. Introduction

Film formation from a polymer latex is a complicated, multistage phenomenon. Opinion is divided as to the exact mechanisms that underpin the transformation from a colloidal aqueous dispersion to a continuous polymer layer. However, most workers agree that the process can be divided into a number of discrete steps. Many recent publications[1–3] suggest four distinct stages separated by three transitions. In this and most other descriptions, Stage I corresponds to the wet initial state. Evaporation of water leads to Stage II in which the particles first come into contact with each other, forming a close-packed array with water-filled interstices. During the transition to the next stage, loss of this interstitial water coincides with particle deformation and compaction. The mechanism by which particle deformation and water loss are linked is still the subject of debate. Stage III indicates a dense array in which individual particles retain their identity. Finally, diffusion across particle–particle boundaries leads to a homogeneous, continuous material (with no internal solid–solid interfaces) that defines Stage IV. This transition from III to IV can only occur above the glass transition temperature (T_g) of the polymer. An idealized schematic summarizing the entire process is shown in Figure 1.

Polymer latex is an important industrial product, and its film formation process has therefore been the subject of much theoretical and experimental attention. However, direct, conclusive evidence in support of the above model is somewhat lacking. Many studies of the individual stages, utilizing a variety of different techniques, have been published. For example, Haas-Bar Ilan and co-workers[4] have used vitreous preparation transmission electron microscopy (TEM) to investigate concentrated aqueous dispersions indicative of late Stage I polystyrene latex. Atomic force microscopy (AFM)[5] has been utilized recently to observe the surface topography and packing of early Stage III poly(butyl methacrylate) (PBMA) systems. The molecular inter-

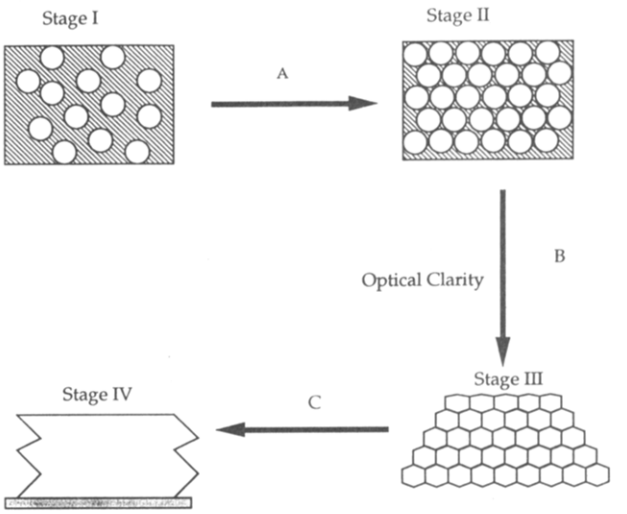

Figure 1. Idealized representation of the four basic stages of polymer latex film formation.

diffusion phenomena of late Stage III and Stage IV have also been extensively studied by such techniques as small-angle neutron scattering (SANS)[6–10] and nonradiative energy transfer (NET).[11–14] The time dependence of particle deformation occurring at the surface of a PBMA latex during the Stage III to IV transformation has been measured with AFM by Goh and coworkers.[15] A variety of TEM and scanning electron microscopy (SEM) methods have predominantly been employed to investigate Stage III and IV microstructure. Examples of these include the replica freeze fracture TEM work of Wang *et al.* and Roulstone *et al.*,[16] the stained TEM observations of Joanicot and co-workers,[8] the replica SEM of Vanderhoff,[17] and the direct SEM studies of El-Aasser.[18]

Comprehensive analyses spanning all four stages are less common. Chevalier *et al.*[19] have bridged the gap of several stages by using a combination of TEM and SANS. They report the observation of long-range order (colloidal crystallinity) in the concentrated dispersions of late Stage I PBA/PS copolymer latex. The important

[⊗] Abstract published in *Advance ACS Abstracts,* March 1, 1995.

0024-9297/95/2228-2673$09.00/0

Stage II state and the mechanisms of the II to III transition, however, are not examined in detail. In another SANS study, particle deformation occurring during the transition from Stage II to III was studied by Crowley and co-workers.[7] They observed the development of a polyhedral foam-type structure as the volume fraction of solids rose above that of close-packing as a result of the evaporation of solvent.

On the theoretical side of latex film formation, pioneering work was published by Brown in 1956.[20] He proposed that the overcoming of mutual particle–particle repulsions and particle deformation during the Stage II to III transition are both driven by the capillary action of interstitial solvent. Alternatively, Vanderhoff *et al.*[17] suggest that these processes are driven by polymer–water interfacial tension. In this publication, Laplace's equation is used to show that matter is pushed under a pressure gradient from the center of the particle to the contact area. One other opinion is that held by Sheetz.[21] His theory involves the formation of a surface layer of coalesced particles formed by capillary action during Stage II and III. This layer constitutes a barrier through which the remaining water must diffuse and which leads to an osmotic pressure that causes the compaction of particles beneath the barrier.

For the purposes of application as a paint or adhesive, the most important latex property is its minimum film-forming temperature (MFFT). As has already been pointed out elsewhere,[22] MFFT is often ill-defined and poorly understood. A quick, convenient, empirical method for its determination was first developed in 1960 by Protzman and Brown.[23] This commonly used technique, referred to as the "bar test", entails spreading the wet latex onto a metal bar having a temperature gradient along its surface. The temperature at the point along this bar at which the latex becomes optically clear and attains mechanical integrity is defined as its MFFT. This optical clarity is achieved in a latex only when the size of pores or voids is well below the wavelength of visible light. Therefore, the bar test is most likely an indication of the minimum temperature needed for the transition from Stage II to III. It does not, however, provide any information about the kinetics of this or any of the other transitions.

In normal use as a paint or adhesive, a latex is applied in its wet state and allowed to dry and film-form under ambient pressure conditions and at room temperature. Conventional electron microscopy, used in the studies already discussed, has always precluded the direct study of "wet" systems such as Stage I and II latex. This is because these microscopies impose drastic drying and sample preparation procedures. Environmental SEM (ESEM), on the other hand, has the specialist capability of submicron imaging of nonconducting "wet" specimens without disruption of microstructure or danger of preparation artifacts. In this work, we have used a combination of multiple-angle-of-incidence ellipsometry (MAIE) and ESEM to follow the evolution of latex films from Stage I through to Stage IV. Both MAIE and ESEM allow the conditions of "normal" application to be replicated during analysis and are therefore ideal techniques for the study of latex film formation. To our knowledge, MAIE and ESEM have never before—either alone or in conjunction—been used in the study of polymer latices.

In our study, we have determined the microstructure and optical characteristics of latices in each of the four stages of film formation. Based on our experimental observations, we shall clarify and modify the existing four-stage model, casting particular insight into the Stage II to III transition. Additionally, our interpretation rigorously describes the microstructure at the onset of film formation as conventionally defined by the bar test. Furthermore, we determine the role of the polymer viscosity in determining the kinetics of the film formation process.

Table 1. Latex Chemical Compositions[a] and Physical Characteristics

	chemical composition			
latex no.	MMA (mol %)	2-EHA (mol %)	diam (nm)	T_g (°C)
1	74.8	24.3	566.2	62
2	54.3	44.8	286.3	13
3	48.8	50.3	303.2	1
4	42.9	56.2	554.2	−5
5	30.0	69.1	356.1	−28

[a] All latices contain 0.9% methacrylic acid.

II. Experimental Procedure

(i) Materials. We studied a series of latex compositions, all based on a copolymer of methyl methacrylate (MMA) and 2-ethylhexyl acrylate (2-EHA). The glass transitions of the copolymers ranged from 245 to 335 K, depending on the proportion of MMA and 2-EHA. Particle size (determined with photocorrelation spectroscopy) and glass transition temperature T_g (determined with differential scanning calorimetry of dried latex) are listed in Table 1 for each of the latex compositions used in this work.

The latices were prepared via a two-stage emulsion polymerization process starting with a seed latex made from 10 mol % of the monomer. Polymerization of the copolymers (the compositions of which are given in Table 1) was achieved by thermal initiation. Ammonium persulfate (0.3 mol % of the monomer) was heated with the monomers at 85 °C. Stabilization and emulsification were achieved with both nonionic and anionic surfactants. A cellulose ether was used as a protective colloid. All latex compositions were approximately 55 wt % in water.

Note that the latices have similar particle sizes but very different T_g values. The polymer in latex 1, which has a relatively high T_g, is a glass at room temperature. Latex 2, which is just above its T_g at room temperature, will have a higher viscosity than latices 4 and 5, which have much lower values of T_g. This range of materials enables us to study the effect of polymer viscosity on the stages and kinetics of film formation.

(ii) Multiple-Angle-of-Incidence Ellipsometry. Ellipsometry requires a planar surface. To achieve such a surface consistently, latex solutions were placed on silicon single-crystal substrates and spun-cast at 1800 rpm for approximately 2 s. This procedure created a smooth, wet surface. The latex was deposited on the roughened side of the silicon substrate so as to eliminate reflection from the latex/substrate interface during ellipsometry. We defined the end of the spinning process as the starting point in the evolution of the latex coating, and we designated it as time $t = 0$. Immediately following spinning, we placed the sample on the stage of the ellipsometer and commenced analysis. We performed a series of scans, each lasting between 1 and 2 min, on each of the latex compositions listed in Table 1. At the completion of coalescence, ESEM of cross-sections revealed thicknesses of the layers in the range of $(4-6) \times 10^{-5}$ m.

All of the experiments described here were performed on a Jobin-Yvon Uvisel phase-modulated spectroscopic ellipsometer.[24] In a typical scan, we measured the ellipsometric angles (ψ, the amplitude attenuation, and Δ, the phase difference between the s and p waves) at 0.05° increments in the angle of incidence, ϕ_i, using a fixed wavelength of polarized light (λ = 413.3 nm). Ellipsometric angles[25] are defined by the equation for ellipticity, ϱ:

$$\varrho = \frac{r_p}{r_s} = \tan(\psi)\exp(i\Delta) \qquad (1)$$

where r_p and r_s are respectively the Fresnel reflection coefficients parallel and perpendicular to the plane of reflection. The refractive indices N_1 and N_2 may be complex, consisting of a real component (the refractive index n) and an imaginary component (the extinction coefficient k). For a planar interface between an isotropic, homogeneous, nonabsorbing material (with a complex refractive index of N_2) and a similar ambient of index N_1, the coefficients are functions of ϕ_i and the angle of refraction, ϕ_r. The reflection coefficients are given by

$$r_p = -\frac{N_2 \cos \phi_i - N_1 \cos \phi_r}{N_2 \cos \phi_i + N_1 \cos \phi_r} \tag{2}$$

and

$$r_s = \frac{N_1 \cos \phi_i - N_2 \cos \phi_r}{N_1 \cos \phi_i + N_2 \cos \phi_r} \tag{3}$$

We conducted our measurements around the Brewster angle, ϕ_B, of the latex, defined as the angle of incidence at which $|r_p|^2$ is a minimum. The refractive index of one material can be calculated at a given angle of incidence[26] from the ellipticity:

$$N_2 = N_1 \tan \phi_i \left[1 - \frac{4\varrho}{(1+\varrho)^2} \sin^2 \phi_i\right]^{1/2} \tag{4}$$

when the ambient is transparent and so $N_1 = n_1$. For a nonabsorbing, nonscattering interface (i.e., $k_1 = k_2 = 0$), ψ goes to a minimum of zero at the Brewster angle, making $\varrho = 0$. Equation 4 then reduces to the well-known result that $\tan(\phi_B) = n_2/n_1$. A thorough discussion of the theory of ellipsometry can be found elsewhere.[25,26]

Although it is possible to determine N for a material analytically from a *single* measurement of ϱ, we have taken *several* measurements. This method overdetermines the analysis (eq 4), but it has an important benefit: Several values of ϱ at varying angles compensate for errors in a single point.

As is apparent from eq 4, a plot of the ellipsometric angles as a function of ϕ_i yields information about the refractive index of the materials at an interface. The ellipsometric angles are especially sensitive to the optical constants of a material near the Brewster angle. The amount of curvature in ψ near ϕ_B is related to the extinction coefficient, k. For instance, when ψ goes through a sharp minimum, k is low; when the curvature in ψ is gradual near the principal angle, k is larger. Likewise, the slope of Δ indicates the extinction coefficient. A sharp change in Δ corresponds to low k, whereas, a more gradual change corresponds to larger k. The two main contributions to the extinction coefficient are optical absorption and scattering.[26] Optical absorption arises from any physical mechanism that changes the frequency of light. Scattering can result from internal interfaces (such as voids and inclusions) and rough surfaces.

(iii) ESEM. So-called "natural", "wet", "low pressure",[27] or "environmental" SEM instruments are being used in a variety of applications where flexible observation conditions are required. Environmental SEM (ESEM)[28] is one of the more widely used of these specialist techniques. Samples are imaged in the presence of water vapor or some other auxiliary gas such as nitrogen. By differential pumping, the observation chamber can be held at pressures up to 25 torr, while the gun and column remain at 10^{-6}–10^{-7} torr. These gradients are manufactured by a series of pressure-limiting apertures (PLAs) and separate pumping units for each zone (Figure 2). With short working distances (~2–5mm) a significant proportion of the electron beam is retained within the probe volume, and scattering is referred to as oligo, as opposed to plural.[29] Conventional high-vacuum scintillation-based detectors cannot be used in such circumstances. Instead, the presence of a gas in the chamber is utilized in the so-called "environmental secondary" or "gaseous" detector (ESD/GD).[30] An electrode is biased with respect to the sample surface, and, depending on the magnitude and polarity of the resultant field, different charged species are accelerated through the gaseous environment. Cascade amplification of the signal arising from the specimen yields high signal to noise ratio, and an image is reconstructed from the measured electrode current. The positive ions produced in this cascade process may then be used to neutralize excess negative charge that builds up at the sample surface. Hence, electrically insulating specimens do not need to be coated with a conducting layer in order to prevent image distortion.

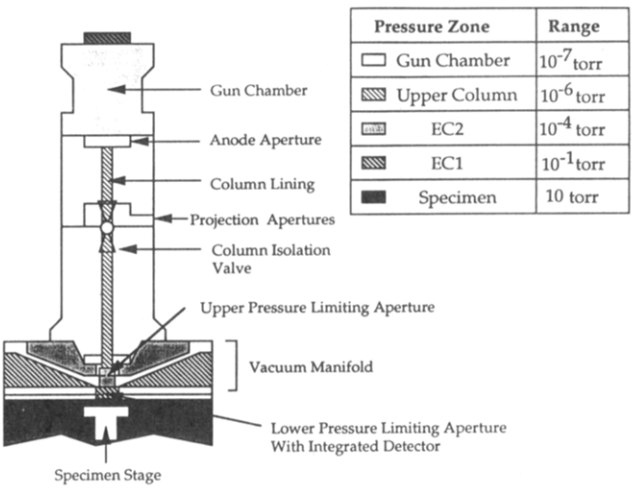

Figure 2. Schematic of the ElectroScan ESEM (Model E-3), showing the differential pressure zones.

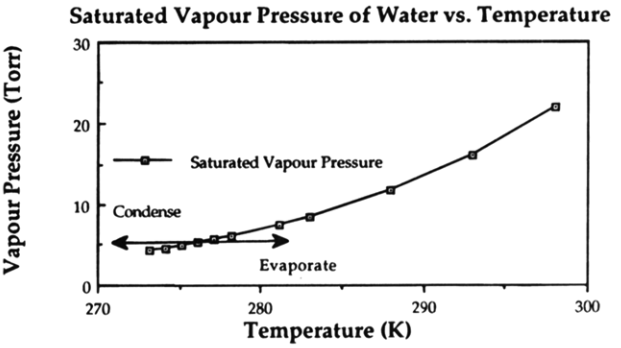

Figure 3. Saturated vapor pressure of water as a function of temperature.

By controlling the temperature of the sample and using water vapor as the imaging gas, condensation and evaporation conditions can be produced. This process is demonstrated in the plot of saturated vapor pressure of water vs temperature shown in Figure 3. The data illustrate that at a temperature of 2–3 °C, an equilibrium vapor pressure of water is obtained at about ~5.6 torr. Dehydration can be inhibited by the correct pumpdown procedure, i.e., the replacement of normal air in the chamber with an imaging gas such as water vapor, and wet samples can therefore be observed in their "natural state".[31] This flexibility in observation environment also means that microstructural changes, for example, those occurring during the film formation of polymer latex, can be studied *in situ* and in real time.

Our experimental procedure for observing such changes was as follows. We inserted a wet latex film into the specimen chamber with its temperature set at ~4 °C. The chamber was then partially evacuated, and the mixed atmosphere progressively replaced with water vapor. During this process we observed no significant loss of sample moisture. We set the correct equilibrium imaging pressure (3–6 torr) and then observed the surface of the latex film in various stages of dehydration during the film formation process. We accelerated Stages II–IV when necessary by increasing the temperature of the sample stage to ~20 °C for varying times.

(iv) Drying Experiments. Samples were prepared in the same way as for ellipsometry. Immediately after spin-deposition, we placed a sample on a scale with a digital read-out. The sample was allowed to dry at room temperature in still air. We recorded the sample weight every 15 s until there

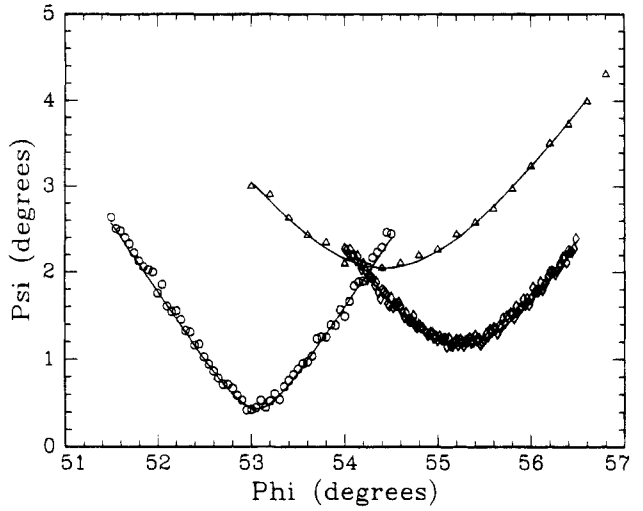

Figure 4. Typical angular ellipsometry scans for latex no. 3. Ellipsometric angle, ψ, *vs* angle of incidence for three different times after film casting. Data are shown for three different scans: (o) 400 s; (△) 1400 s; (◇) 2540 s. Solid lines are the curves of best fit to a model for a semi-infinite solid.

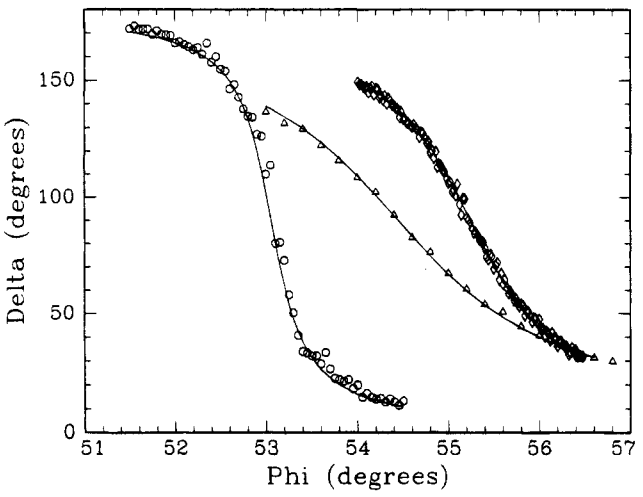

Figure 5. Typical angular ellipsometry scans for latex no. 3 Ellipsometric angle, Δ, *vs* angle of incidence for three different times after film casting. Data are shown for three different scans: (o) 400 s; (△) 1400 s; (◇) 2540 s. Solid lines are the curves of best fit to a model for a semi-infinite solid.

was no discernible change in the weight over a period of several minutes.

III. Results

(i) Optical Characterization. Some typical angular scans of latex 3 are shown in Figures 4 and 5. Ellipsometric angles (ψ and Δ) are plotted as a function of the angle of incidence for three different times after film deposition, and the curves of best fit to the data are overlaid. One scan (at 400 s) was performed prior to the onset of optical clarity and when the film was noticeably wet (Stage I). The second scan shown (1400 s) was performed shortly after the onset of optical clarity. The third one (2540 s) was obtained after the film had aged for an additional 1140 s. Qualitatively, the trends shown in Figures 4 and 5 indicate that refractive index increases with time, but extinction coefficient increases and then decreases again.

We can analyze data such as in Figures 4 and 5 by finding the complex refractive index that yields the best fit of ψ and Δ to eq 4. The error in each component of the complex refractive index (n and k) is about 0.001.

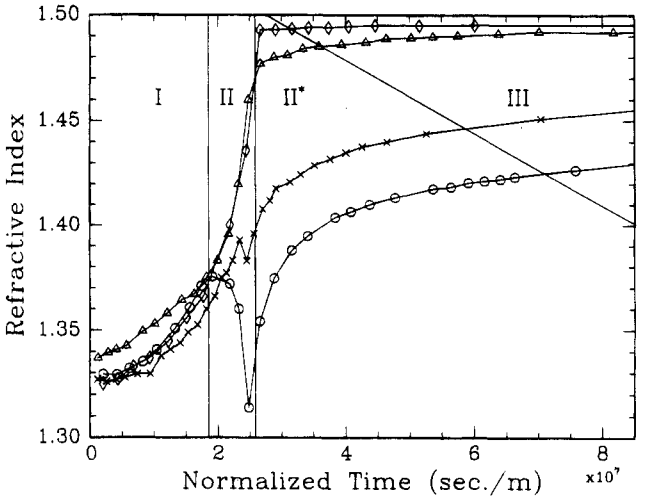

Figure 6. Refractive index as a function of time normalized with respect to final film thickness. Data obtained by fitting the ellipsometric measurements as shown in Figures 4 and 5. The Roman numerals designate the various stages of film formation, and the straight lines mark the transitions between the stages. Data are shown for four film-forming latices: (o) no. 2; (×) no. 3; (△) no. 4; (◇) no. 5.

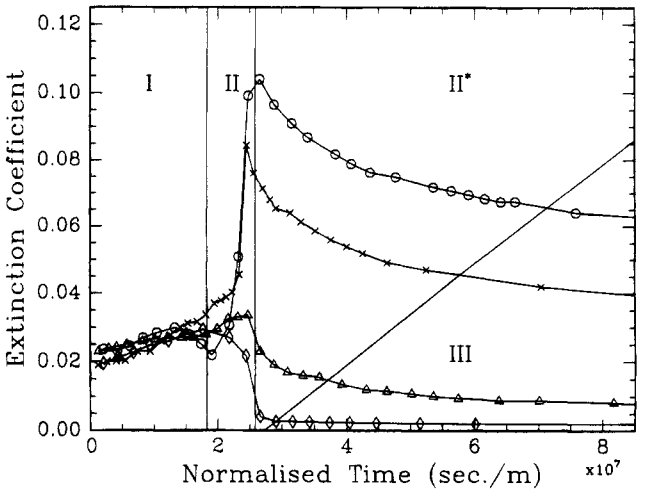

Figure 7. Extinction coefficient as a function of time normalized with respect to final film thickness. Data obtained by fitting the ellipsometric measurements as shown in Figures 4 and 5. The Roman numerals designate the various stages of film formation, and the straight lines mark the transitions between the stages. Data are shown for four film-forming latices: (o) no. 2; (×) no. 3; (△) no. 4; (◇) no. 5.

Refractive indices and extinction coefficients obtained from a series of successive scans are shown in Figures 6 and 7 for latex compositions 2–5. In our experiments, we shall show that the evaporation *rate* of water from a latex is independent of thickness, as has been shown elsewhere.[32] We thus expect the volume fraction of water at a particular time to be proportional to the initial thickness of the wet film. This is because each of the latices are cast onto substrates of the same area and their initial volume fractions of water are similar. In Figures 6 and 7 we have normalized the data by dividing the drying time by the final film thickness. We determined film thickness by examining film cross-sections using ESEM. The normalized time is expected to be linearly proportional to the volume fraction of solids in the drying latex.

In interpreting the refractive index, we draw upon the well-known Lorentz–Lorenz equation. It relates n to $\tilde{N}$, the number of objects (of a size much smaller than λ) per unit volume:

$$\frac{n^2-1}{n^2+2}=\frac{\tilde{N}\alpha}{3\epsilon_0} \tag{5}$$

where α is the real component of the polarizability, and ϵ_0 is the permittivity of free space. Since $\tilde{N}$ is proportional to material density[26] and bearing in mind the relationship in eq 5, we can therefore use n as a probe of material density on a size scale less than 400 nm, realizing that the values we obtain are an average over the volume probed. As such, we interpret values of n less than the index of the bulk polymer as being indicative of air voids within the material.

The extinction coefficient provides very different information. As mentioned previously, k is an indication of the amount of radiation that is absorbed or scattered. Consequently, k is sensitive to such things as voids and rough surfaces. Our measurements yield an effective value of k that, in most cases, is not equivalent to the value in the bulk material. One possible reason for this discrepancy is that the surface of a non-film-formed latex is expected to be rough on the size scale of the particle radius. Azzam and Bashara[25] have presented simulations indicating that although apparent refractive index is rather insensitive to surface roughness, the extinction coefficient increases by approximately 0.03 with a relatively small increase in surface roughness of 10 nm. Additionally, whereas voids larger than λ are not expected to affect n greatly, they are expected to cause scattering and consequently an increase in k. To summarize, it is useful to bear in mind when interpreting our data that n is particularly sensitive to microscopic voids in the latex, and k is sensitive to surface roughness and to interstices and voids of varying sizes.

Most notably in Figures 6 and 7, each of the latex compositions undergoes a significant optical change near a normalized time of 2.7×10^7 s/m. We have observed that this point in time corresponds to the onset of optical clarity in the films and thereby defines film formation according to the bar test. Note that the normalized time for this optical change is the same for all of the film-forming latices studied, even though MFFT and T_g vary widely among them.

The exact manner in which the complex refractive index changes around a normalized time of 2.7×10^7 s/m (for instance, the magnitude of the increase or decrease) *does* vary with MFFT and T_g, however. Specifically, the refractive index (Figure 6) of latex 2 decreases abruptly near this time and then increases once more. The refractive indices of latices 4 and 5, in contrast, increase substantially (by more than 0.1). The index of latex 3 displays an intermediate behavior. The index drops slightly (but much less than that of latex 2), and it then increases, but much more gradually than for latices 4 and 5. At normalized times greater than about 3.0×10^7 s/m, the refractive index increases the most in latex 2 and the least in latex 5, with latices 3 and 4 showing intermediate trends.

The extinction coefficient (Figure 7) of latex 2 increases sharply near a normalized time of 2.7×10^7 s/m. Latex 3 follows a similar trend, but the magnitude of the increase is less. The extinction coefficient of latex 5 decreases abruptly at this time. Once more, latex 4 displays an intermediate trend. There is a slight increase in extinction coefficient near a normalized time of 2.7×10^7 s/m followed by a gradual drop. Above this normalized time, the k of latex 2 changes the most and latex 5, the least, in a trend similar to that seen in n in the previous figure.

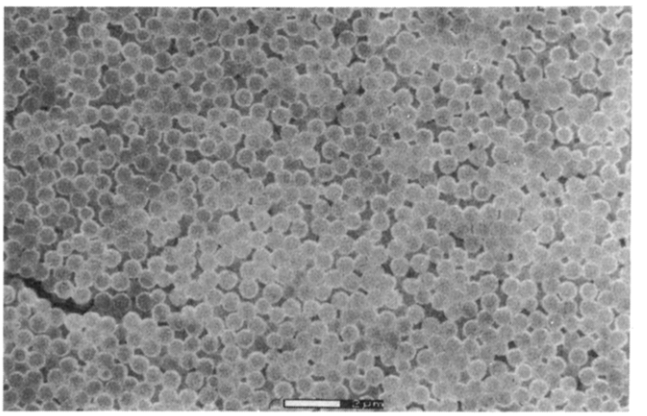

Figure 8. ESEM micrograph showing the surface of a hydrated Stage II non-film-forming latex (no. 1); magnification bar = 2 μm.

(ii) Microstructural Evidence. The following results detail ESEM microstructural observations. We selected three latices (nos. 1, 2, and 4) with very different values of T_g, but with similar particle sizes. Latex 1, since it is below its MFFT at room temperature, is non-film-forming. Latex 2 is expected to have a much higher viscosity in comparison to latex 4, and we shall refer to latex 2 as "hard" and latex 4 as "soft".

It is also useful at this point to note that when we refer to the Stage II latices as being "wet" or "hydrated", some water has in fact been removed from the surface to obtain better images. The surface in this sense is therefore partially dehydrated although the bulk is still completely "wet". Dry latices (Stage III of IV) were observed with a small amount of water condensed on the surface during imaging. This had the effect of enhancing edge contrast, as will be described elsewhere.[33]

(a) Non-Film-Forming Latex (No.1): We find that the surface of a hydrated latex can be successfully imaged in the ESEM under "wet" conditions. We have observed that the monodisperse particles of this high-T_g (~60 °C) latex are randomly distributed, with very little tendency to order in this "wet" state. As shown in the micrograph of Figure 8, the hydrophilic shells of the latices retain their moisture and display a bright contrast "halo".[33] We also observed that the particles remained physically distinct and that no deformation occurred (Figure 8). Since the particles are in contact but have water in their interstices, we conclude that the latex is in Stage II.

When these films were dried, a similar microstructure to the "wet" case was observed. Notably, the particles retained their individual identities although intimate contact had been established. A great deal of porosity was still clearly apparent, and the samples, when viewed optically outside the microscope, appeared opaque despite their dryness. The electron micrograph of Figure 9 demonstrates some of these points. As before, a small amount of water was condensed on the sample surface to enhance edge contrast. The major difference between the "wet" state of Figure 8 and this "dry" state is the occurrence of isolated multiparticle clusters (see for example cluster A). Within such groupings a limited amount of ordering has been initiated, and regular triangular, diamond, pentagonal, and hexagonal pores can be seen. This pore regularity is a direct consequence of particle rigidity. Note that since the latex does not film-form, it never attains Stage III. Thus we never observe particle deformation or the formation of a densely packed array.

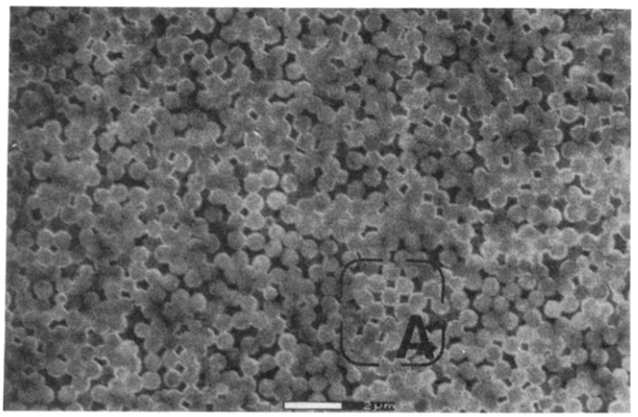

Figure 9. ESEM micrograph showing the surface of a dehydrated post-Stage II non-film-forming latex (no. 1), held at 20 °C for ~1 h; magnification bar = 2 μm.

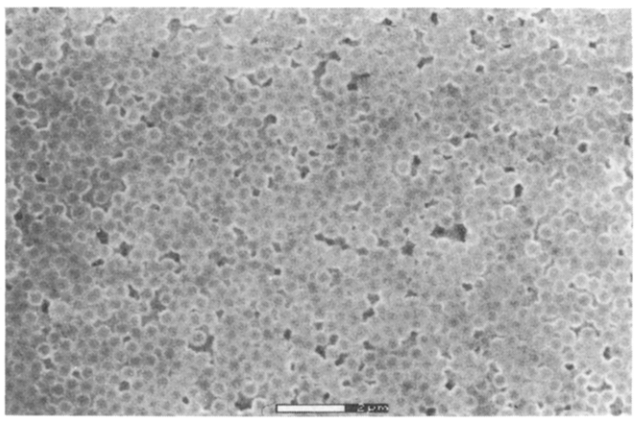

Figure 10. ESEM micrograph showing the surface of a hydrated Stage II hard film-forming latex (no. 2); magnification bar = 2 μm.

(b) Hard Film-Forming Latex (No.2): While still in the hydrated state we noted that the particles of latex 2 remained physically distinct and undeformed. The wet films appeared opaque when studied optically and contained a great deal of porosity when viewed in the ESEM. The electron micrograph of Figure 10 is an example of such a Stage II hydrated latex. The particle boundaries are still clearly visible except in a few isolated areas where premature dehydration has occurred.

When this latex was dehydrated in the ESEM and allowed to film-form for approximately an hour at room temperature, much of the large-scale porosity was seen to disappear. Such films possessed mechanical integrity, appeared optically transparent outside the microscope, and—by the conventional definition—had therefore film-formed. We observed that rearrangement and packing of the particles into ordered arrays did occur, signaling that Stage III had been reached. Individual particle identities were retained long after the attainment of Stage III. The electron micrograph of Figure 11, when seen in contrast to Figure 10, demonstrates some of these points. Within this typical Stage III latex, packing in the matrix is nonuniform.

(c) Soft Film-Forming Latex (No. 4): When the partially dehydrated surface of a "wet" (Stage II), soft (for example no. 4) latex is examined, extensive particle deformation can be seen immediately upon attainment of particle–particle contact. We observed that such films were still optically opaque; accordingly, their microstructure contained a large amount of porosity. The electron micrograph of Figure 12a,b shows such a

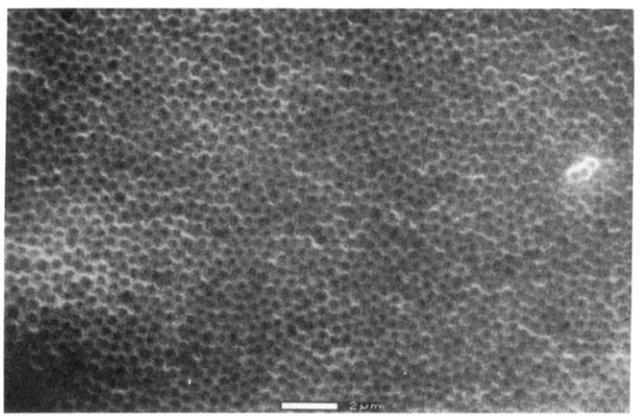

Figure 11. ESEM micrograph showing the surface of a dehydrated Stage III hard film-forming latex (no. 2), held at 20 °C for ~1 h; magnification bar = 2 μm.

Stage II soft latex after excess surface water has been removed. These particular micrographs were taken at a temperature of ~5 °C in order to inhibit imminent film formation. Particles within clusters can be seen to have deformed to quite a large extent in minimizing the polymer surface area. In certain cases, cluster B for example (expanded in Figure 12b), four particles have individually deformed to come together at right angles.

In such a soft latex, the transition from Stage II through Stage III to Stage IV is very rapid. Upon dehydration and exposure to a temperature of ~20 °C, all particle identity rapidly disappeared. We observed continuous films, characteristic of Stage IV latex, after a very short period. An example of such a surface is shown in the electron micrograph of Figure 13. No individual particles can be seen, and the only topographical features are due to defects and possibly impurities.

(iii) Drying Rate. Data from drying experiments on three of the latex compositions are shown in Figure 14. Water loss (mass loss per unit area) is plotted against the time elapsed since the deposition of the latex. In all of the experiments, the water loss initially increases linearly with time. The slope of curves such as these indicate that the rate of water loss in the latex is, on average, $(3.8 \pm 0.2) \times 10^{-5}$ kg m^{-2} s^{-1}. This value, which is independent of film thickness, compares favorably with the reported evaporation rate of water in still air at room temperature, 3.6×10^{-5} kg m^{-2} s^{-1}.[32] In theories of drying, this initial stage is called the constant rate period. Evaporation takes place from the water/air interface at the material's surface. After this constant rate period, there is a falling rate period in which the drying rate decreases to zero. The falling rate period is believed to be the result of slowed diffusion of water vapor through a dry surface layer after the water/air interface (the drying front) recedes from the surface. The inception time of the falling rate period depends on film thickness, occurring at a later time for thicker films. In Figure 14 latices 2 and 5 have similar thicknesses, and so the constant rate period and falling rate period occur over nearly identical times. These results support our earlier arguments in normalizing the drying times.

Since we have measured the rate of water loss in drying latex films and since we know that the latex solutions are initially 55 wt % solids, we can calculate the volume fraction of water in the films (assuming no air porosity) as a function of time. This analysis provides a rough estimate of the amount of water in the

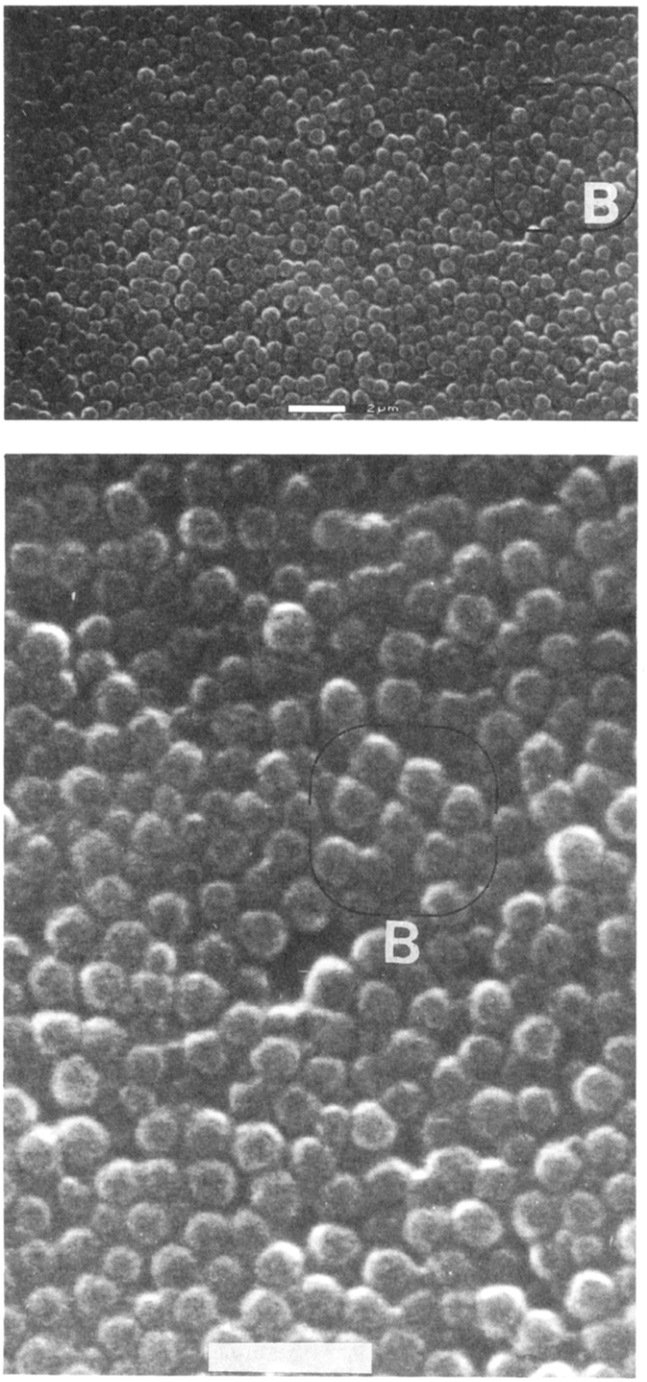

Figure 12. ESEM micrographs showing the surface of a hydrated Stage II soft film-forming latex (no. 4): (a, top) normal magnification (bar = 2 μm); (b, bottom) expanded view (bar = 2 μm).

films at the onset of film formation. We estimate that at the normalized time of 2.7×10^7 s/m, there is less than 15 volume percent water. Furthermore, we have made the qualitative observation that the onset of the falling rate period correlates with the appearance of optical clarity near the edge of a sample; the onset of the plateau region correlates in time with the completion of film formation.

IV. Discussion

We shall discuss the data in Figures 6 and 7 and in the ESEM micrographs in terms of the four stages of film formation outlined in the Introduction. By correlating optical and microstructural data, we isolate and define each of the stages. As a guide to our discussion,

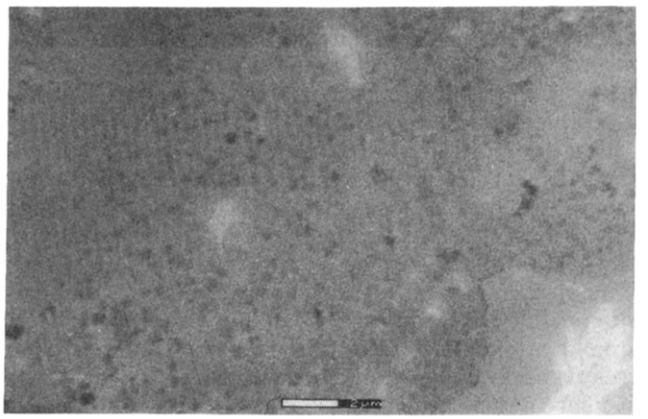

Figure 13. ESEM micrograph showing the surface of a dehydrated Stage IV soft film-forming latex (no. 4), held at 20 °C for ~1 min; magnification bar = 2 μm.

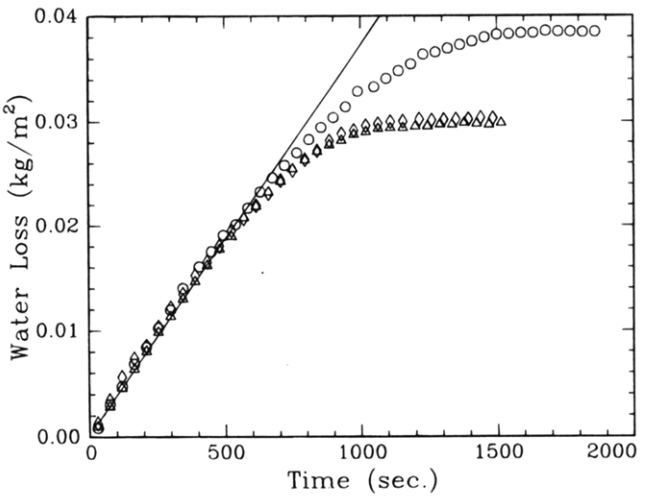

Figure 14. Water loss as a function of time after casting for latices 1, 2, and 5 (non-film-forming, hard and soft, respectively): (o) no. 1; (△) no. 2; (◇) no. 5.

we have drawn lines on Figures 6 and 7 to demarcate the transitions between the various stages. As our discussion proceeds, it will become clearer how we determined the positions of these lines.

Because the wet latex is highly turbid, ellipsometry is sensitive only to the top surface. This surface in Stage I is initially expected to consist primarily of water. Accordingly, the initial refractive index (for all latex samples) is close to 1.33, the value for water. Our measurements thus support the notion that the surface of the latex initially consists only of the aqueous solvent and that the latex is in Stage I. We have labeled this time period with an "I" on Figures 6 and 7 to indicate the stage.

As a latex makes the transition to Stage II via the evaporation of water, particles begin to emerge from the surface. This has the effect of raising the material density at the surface, which in turn increases the observed refractive index. (In similar work, Meeten *et al.* have found that refractive index (determined with refractometry) of Stage I latex increases with solids concentration.[34]) The particles emerging from the water create a rougher surface, and the apparent extinction coefficient therefore rises simultaneously. Supporting this argument is our finding that in all of the latices studied, both n and k increase linearly with time at normalized times between 0 and 2.0×10^7 s/m. Meanwhile over this same time period, the volume fraction of particles is increasing from about 55 to 80 volume percent.

Eventually the particles come into contact with each other, and the latex thereby reaches Stage II. We suggest that the onset of Stage II is signaled by changes in the complex refractive index occurring at a normalized time near 2.0×10^7 s/m. At this point, identified with a line marking the onset of Stage II on Figures 6 and 7, both refractive index and absorption coefficient show a change in slope. The critical solid content at which contact occurs is dependent upon the configuration of the packing. For example, in a face-centered cubic array of rigid, monodisperse spheres, the maximum volume fraction is 0.74. If, however, the particles are able to deform after their initial contact, then greater packing densities are possible. Our drying rate measurements predict that at this normalized time, the latex consists of less than about 20 volume percent water (corresponding to 80 volume percent solids). This rather high solids content indicates particle deformation in all of the film-forming latices, even before Stage III. We found that evaporation continues at a constant rate during this time and does not enter the falling rate period. This finding supports the notion of particle deformation keeping the water/air interface at the latex surface.

We will now consider as a separate case, the *non film-forming* latex 1, which is below its T_g at room temperature. Recall that no particle deformation is observed with ESEM in either its wet (Figure 8) or dry state (Figure 9). This is clearly demonstrated in the ordered multiparticle clusters of Figure 9, where intimate contact has been established and regular enlarged interstices exist. We find that the optical properties of latex 1 change substantially and abruptly at a normalized time of only about 0.5×10^7 s/m. (Our data are not shown.) The effective refractive index falls, and the extinction coefficient rises. Our measurements of drying rate indicate that at this point in time the latex consists of approximately 40 volume percent water. Since a random packing of rigid particles is expected to be around 60 volume percent solid,[35] we attribute the change in optical characteristics to the level of water in the latex dropping below the *top* surface of the particles after they have come into contact. That is, we see optical evidence for the drying front (the water/air interface) receding into the latex. Since the particles do not deform, voids and surface roughness develop during the process. Then the light is not reflected from the wet surface; instead the reflection is from dry particles. This rough surface has a low effective refractive index and a high extinction coefficient. Note that we observe this optical change when there is still a large amount of water in the latex.

To summarize, we find that since particles of a non-film-forming latex cannot deform, a rough, dry surface develops at a relatively low solids content as the drying front recedes into the latex and away from its outer surface. In a film-forming latex, however, the particles deform to achieve a denser packing. A partially wet surface is consequently maintained at much higher solids content. This difference between the film-forming and non-film-forming latices supports the suggestion of a "self-regulating" drying mechanism. Sheetz (extending ideas proposed by Brown) hypothesized that there is a capillary force normal to the film that deforms and compacts the particles. This compaction and deformation of the wet particles (as seen in Figure 12) "squeezes" water to the top surface, thereby keeping the particles submerged. Such a mechanism is not possible with the rigid particles of a non-film-forming latex.

Over the time period that follows the onset of Stage II, we find that the conventional description of film formation consisting of four stages is inadequate in describing our observations. Conventional thought suggests that the transition from Stage II to Stage III is the result of *simultaneous* water evaporation, particle deformation, and the attainment of optical clarity. We find that the transition between Stage II and Stage III is not continuous but contains an intermediate stage. We suggest that in most latex systems, an intermediate stage exists in which optical clarity is achieved after loss of most of the interstitial water and after partial particle deformation. However, unlike in Stage III, the particles in this stage are not completely dry and not yet compacted in a dense array. We shall refer to this newly identified intermediate stage as II*.

During the transition between Stages II and III, the particles pack more densely together as water evaporation proceeds. We suggest that particles of latex 2 (which is close to its T_g at room temperature) are unable to deform substantially as water evaporates from the sample. As a result, when the drying front recedes from the surface, air voids develop within the array of particles, leading to a marked increase in surface roughness and an accompanying increase in the extinction coefficient. The observed decrease in the effective refractive index likewise supports the concept of void formation during the transition. We propose that these optical and microstructural changes, which occur near a normalized time of 2.7×10^7 s/m, signal the onset of Stage II* and have therefore labeled it as such on Figures 6 and 7. Interestingly, though, despite the presence of voids, there is sufficient polymer/polymer contact to enable optical clarity in the latex. Note that particles do not have to be coalesced in order to create an optically clear film. The voids between the latex 2 particles are much less than the wavelength of the incident light. This is not surprising considering that the particle diameters and the wavelength are roughly the same (about 400 nm).

Soft particles (such as latices 4 and 5) by contrast are able to deform simultaneously as water evaporates. This ease of deformation, resulting from a relatively low viscosity, is clearly demonstrated by the flat edges between particles while still in Stage II (Figure 12). With continued water evaporation and the receding of the drying front, a rough surface and voids do not form and so the extinction coefficient drops near the time labeled as II*. As a greater fraction of the latex consists of polymer and less consists of water, there is a simultaneous increase in material density that leads to a rise in refractive index.

Latex 3 has an intermediate glass transition temperature (intermediate viscosity) and as a result displays a behavior intermediate to latices 2 and 4. The refractive index decreases briefly after the transition to II*. We suggest that this moment corresponds to the temporary appearance of air voids in the latex created by the evaporation of water. The latex deforms to eliminate these voids at a fast rate, however, and the latex density therefore increases sharply. At the same time, the extinction coefficient increases as a result of some surface roughness. The particles rapidly deform and flow to create a smoother surface (consistent with the observed increase in density), and so the extinction coefficient then falls sharply.

Why do the abrupt changes in optical properties and the onset of optical clarity occur at nearly the same normalized time for all the film-forming latices? The answer seems to be that there is a critical solids content

which corresponds to the void size being able to drop well below the wavelength of light. The attainment of this condition is governed by the evaporation of water in conjunction with particle deformation. (The exact cause-and-effect relationship between the two cannot be determined from this study.)

The microstructural evidence provided by ESEM is in agreement with these arguments. The electron micrographs of Figures 10 and 11 show latex 2 on either side of Stage II*. The "wet" (end of Stage II) microstructure of Figure 10 displays a large amount of interstitial void space, consistent with a relatively high extinction coefficient and low effective refractive index. The "dry" (start of Stage III) microstructure of Figure 11 provides further evidence that the majority (but not all) of the porosity has been eliminated and a dense array has formed. This microstructure has been achieved by particle rearrangement and deformation, and it is consistent with our finding of higher refractive index and lower extinction coefficient. However, microporosity, not easily observed with ESEM, must still exist since individual particles clearly retain their identity.

Whereas Stage II* latex is characterized as having air voids between particles, Stage III is described as a densely packed array. Bearing this in mind, we suggest that the rate of the transition from Stage II* to Stage III is dependent on the glass transition of the latex. In a soft latex (with a low T_g, such as no. 4), the polymer has a relatively low viscosity, and a relatively high particle packing density is achieved in Stage II*. Consequently, Stage III is reached almost immediately after Stage II*. So rapid is this transition that on the time scale of the ESEM experiments, at least, a densely packed array of particles cannot be observed. Figure 13 shows that a continuous polymer layer is formed soon after the transition, in support of the rapid attainment of optical properties indicated by MAIE. We suggest that the limiting step in the attainment of Stage III in this latex is the evaporation of water. In a hard latex (such as no. 2), on the other hand, it takes much longer to achieve the array of Stage III. This fact allows us to isolate Stage III with ESEM (Figure 11). Unlike the softer latex, the hard latex contains a large amount of porosity at the onset of Stage II*, and its rate of viscous flow is quite slow. All of the water is expected to be evaporated long before the attainment of Stage III. This fact implies that particle deformation during this stage is driven by the energy savings from the reduction of the polymer/air surface area. Clearly, the density and microstructure of the latex are time-dependent, in agreement with what is expected for a "dry sintering" mechanism. An earlier suggestion[36] that elastic deformation driven by adhesion forces (a mechanism that does *not* show a time dependence) causes latex coalescence is not supported by our experiments.

The diagonal lines in Figures 6 and 7, which mark our estimates for the onset of Stage III, illustrate our interpretations. In all of the latices, regardless of T_g, n and k vary with time during Stages II* and III. The values of the complex refractive index of latex 4 approach values of the bulk shortly after the onset of Stage II*. Attributing this observation to the rapid smoothing of the surface and the loss of voids during the transition to Stage III is in direct agreement with our ESEM observations just discussed. Latex 2 has the greatest amount of voids and the greatest surface roughness at Stage II* (explaining its low n and high k), and its optical properties change at the slowest rate, also in support of the ESEM observations.

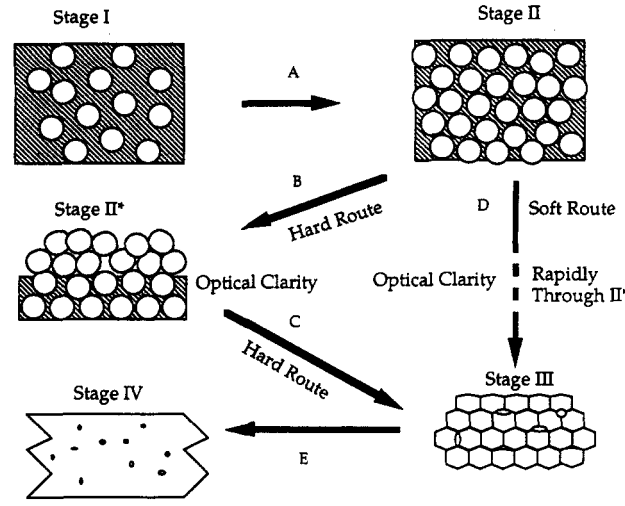

Figure 15. Modified "intermediate Stage II*" model of polymer latex film formation, idealized as in Figure 1.

We have identified the onset of Stage IV using ESEM by observing the elimination of particulate identity. The time until the attainment of Stage IV is dependent on the T_g of the polymer, as is the onset of Stage III. In latex 4 (Figure 13), Stage IV is attained shortly after the transition to Stage III. The transition is too fast to capture with ESEM. In contrast, the harder particles of latex 2 (Figure 11) coalesce on a time scale easily observed with either ESEM or MAIE; Stage IV is not reached until several weeks after Stage III. This finding supports previous work[1] that observed an inverse dependence of interdiffusion rate on the T_g of the polymer.

Figure 1 outlines the conventional view of four stages of film formation linked by three transitions. We suggest in Figure 15 that the intermediate stage of II* is obtained in a latex that is only slightly above its glass transition temperature and is therefore somewhat rigid (latex 2 at room temperature, for instance). In a latex that is well above its T_g, the microstructure passes rapidly from Stage II through Stage II* to Stage III, since the particles deform at a sufficient rate to fill voids left by the evaporation of water. In a soft latex, the evaporation of water is the rate-limiting step in the transition to Stage III.

In addition to the insertion of Stage II*, our Figure 15 contains some minor modifications to the conventional model shown in Figure 1. The figure illustrates that in Stage II we have observed some particle deformation, such as seen in latex 4 (Figure 12). Note also that in illustrating Stage III, Figure 15 shows that in this study a hexagonal array is not attained. The ordering of latex particles (studied in detail elsewhere[5]) is a function of the particle size distribution, ionic strength, choice of surfactant, drying rate, and external shear forces. We attribute the disorder in the particle arrays studied here to the fact that there is not a narrow size distribution.

In closing, we point out that film formation is strongly affected by the choice of surfactant and other chemical additives. Some of our observations, therefore, would not be found in other latex systems. We suggest, however, that our conclusion regarding the general effects of T_g on the kinetics of film formation are generally applicable.

V. Conclusions

The complicated process by which an aqueous, colloidal polymer dispersion evolves into a continuous film

is usually divided into four stages (Figure 1). We have used a combination of multiple-angle-of-incidence ellipsometry and environmental SEM to study *each* of the stages in a series of acrylic latices having similar particle sizes but varying glass transition temperatures. Our analytical techniques allow us to study wet materials in their "natural" state and without special sample preparation.

We find that the onset of film formation occurs at nearly the same normalized time, regardless of the glass transition temperature of the latex. This point occurs during the transition between Stages II and III at an intermediate stage that we call II*. It corresponds to a sharp change in the refractive index and extinction coefficient and accompanies the attainment of optical clarity. We suggest that the *onset* of Stage II* occurs when there is less than about 15 volume percent water in the latex. Film formation takes place when particles gain close contact allowed by the loss of water and particle deformation. As such, in a film-forming latex, the time until the onset of optical clarity (and the attainment of Stage II*) does not depend on the polymer's viscous properties (indicated by T_g).

During Stage II*, a harder latex is unable to deform at a fast enough rate to eliminate the voids created during evaporation and to create a smooth surface. In contrast, a softer latex can deform and flow to eliminate these voids in tandem with the continued loss of solvent. Particle identity is retained during Stage II*, even though optical clarity has been attained.

Densification and microstructural development continue in all film-forming latices after the onset of Stage II*. However, in a softer latex these processes occur rapidly compared to a harder latex, which continues to densify over a period of several days. Similarly, particle identity is destroyed in a much shorter time for the softer latex in comparison to the hard. This is because a polymer close to its glass transition temperature deforms and diffuses at a much slower rate compared to one well above its T_g. Unlike the onset time of Stage II*, the onset times of Stages III and IV *are* dependent on the viscous properties of the polymer. The kinetics of deformation and compaction depend on the viscosity of the particles, which is known to be a function of the polymer's glass transition temperature.

In microstructural development leading to Stage III, there is a negligible amount of water in the harder latices. The driving force for particle coalescence is therefore the reduction of the polymer/air surface area (dry sintering).

In this paper we have demonstrated that ESEM and ellipsometry can be used in a complementary fashion to study the fundamental mechanisms of polymer latex film formation. The need for complicated sample preparation has been eliminated, and in doing so the usual concerns about artifact have been removed. We have been able to study *all* stages of the process *in situ* and in real time, paying particular attention to the experimentally difficult II to III transition. Future work will further utilize the unique "natural" capabilities of the techniques to investigate the effects of hard incompressible inclusions on the process.

Acknowledgment. This work was supported by the DTI, ICI plc, Schlumberger Cambridge Research, and Unilever plc through the Colloid Technology Programme. We thank Drs. R. Cameron, D. Taylor, and P. Sakellariou for useful discussions and advice. ICI Paints in Slough supplied the latices used in this work. We benefited from the technical support of A. Eddy and from a computer program written by F. Nex.

References and Notes

(1) Boczar, E. M.; Dionne, B. C.; Fu, Z.; Kirk, A. B.; Lesko, P. M.; Koller, A. D. *Macromolecules* **1993**, *26*, 5772.
(2) Pekcan, Ö. *Trends Polym. Sci.* **1994**, *2*, 236.
(3) Wang, Y.; Winnik, M. A. *J. Phys. Chem.* **1993**, *97*, 2507.
(4) Haas-Bar Ilan, A.; Noda, I.; Schechtman, L. A.; Talmon, Y. *Macromolecules* **1991**, *33*, 2043.
(5) (a) Juhué, D.; Lang, J. *Langmuir* **1993**, *9*, 792. (b) Wang, Y.; Juhué, D.; Winnik, M. A.; Leung, O. M.; Goh, M. C. *Langmuir* **1992**, *8*, 760.
(6) Hahn, K.; Ley, G.; Schuller, H.; Oberthür, R. *Colloid Polym. Sci.* **1988**, *266*, 631.
(7) Sanderson, A. R.; Crowley, T. L.; Morrison, J. D.; Barry, M. D.; Morton-Jones, T.; Rennie, A. R. *Langmuir* **1992**, *8*, 2110.
(8) Joanicot, M.; Wong, K.; Marquet, J.; Cabane, B. *Macromolecules* **1993**, *26*, 3168.
(9) Linné, M. A.; Klein, A.; Sperling, L. H.; Wignall, G. D. *J. Macromol. Sci., Phys. B* **1988**, *27*, 181.
(10) Linné, M. A.; Klein, A.; Miller, G. A.; Sperling, L. H.; Wignall, G. D. *J. Macromol. Sci., Phys. B* **1988**, *27*, 217.
(11) Kim, K. D.; Sperling, L. H.; Klein, A.; Wignall, G. D. *Macromolecules* **1993**, *26*, 4624.
(12) Pekcan, Ö.; Winnik, M. A.; Croucher, M. D. *Macromolecules* **1990**, *23*, 2673.
(13) Wang, Y.; Winnik, M. A. *Macromolecules* **1993**, *26*, 3147.
(14) (a) Wang, Y.; Zhao, C.-L.; Winnik, M. A. *J. Chem. Phys.* **1991**, *95*, 2143. (b) Zhao, C.-L.; Wang, Y.; Hruska, Z.; Winnik, M. A. *Macromolecules* **1990**, *23*, 4082.
(15) Goh, M. C.; Juhué, D.; Leung, O. M.; Wang, Y.; Winnik, M. A. *Langmuir* **1993**, *9*, 1319.
(16) (a) Wang, Y.; Kats, A.; Juhué, D.; Winnik, M. A.; Shivers, R. R.; Dinsdale, C. J. *Langmuir* **1992**, *8*, 1435. (b) Roulstone, B. J.; Wilkinson, M. C.; Hearn, J.; Wilson, A. J. *Polym. Int.* **1991**, *24*, 87.
(17) Vanderhoff, J. W. *Br. Polym. J.* **1970**, *2*, 161.
(18) El-Aasser, M. S.; Robertson, A. A. *J. Paint Technol.* **1975**, *47*, 50.
(19) Chevalier, Y.; Pichot, C.; Graillat C.; Joanicot, M.; Wong, K.; Marquet, J.; Lindner, P.; Cabane, B. *Colloid Polym. Sci.* **1992**, *270*, 806.
(20) Brown, G. L. *J. Polym. Sci.* **1956**, *22*, 423.
(21) Sheetz, D. P. *J. Appl. Polym. Sci.* **1965**, *9*, 3759.
(22) Dobler, F.; Pith, T.; Lambla, M.; Holl, Y. *J. Colloid Interface Sci.* **1992**, *152*, 1.
(23) Protzman, T. F.; Brown, G. L. *J. Appl. Polym. Sci.* **1960**, *4*, 81.
(24) Jasperson, S. N.; Schnatterly, S. E. *Rev. Sci. Instrum.* **1969**, *40*, 761.
(25) (a) Azzam, R. M. A.; Bashara, N. M. *Ellipsometry and Polarized Light*; North-Holland: Amsterdam, 1987; p 270. (b) *Ibid.*, p 361.
(26) (a) Meeten, G. H. *Optical Properties of Polymers*; Elsevier Applied Science Publishers: London, 1986; p 29. (b) *Ibid.*, p 40. (c) *Ibid.*, p 44.
(27) Farley, A. N.; Shah, J. S. *J. Microsc.* **1991**, *164*, 107.
(28) Danilatos, G. *J. Microsc.* **1991**, *162*, 391.
(29) Danilatos, G. *Scanning Microsc.* **1990**, *4*, 799.
(30) Danilatos, G. *Adv. Electron. Electron Phys.* **1990**, *78*, 1.
(31) Cameron, R. E.; Donald, A. M. *J. Microsc.* **1994**, *173*, 227.
(32) Croll, S. G. *J. Coat. Technol.* **1986**, *58*, 41.
(33) Meredith, P.; Donald, A. M., accepted in *J. Microsc.*
(34) Meeten, G. H.; North, A. N. *Meas. Sci. Technol.* **1991**, *2*, 441.
(35) Levine, M. M.; Chernick, J. *Nature* **1965**, *208*, 68.
(36) Kendall, K.; Padget, J. C. *Int. J. Adhes. Adhesives* **1982**, *2*, 149.

MA946023D